Published in final edited form as:
J Phys Chem B. 2009 May 21; 113(20): 7407–7417. doi:10.1021/jp9010795.

A SPECTROSCOPIC INVESTIGATION OF A TRIDENTATE Cu-COMPLEX MIMICKING THE TYROSINE-HISTIDINE CROSS-LINK OF CYTOCHROME *c* OXIDASE

Adam Offenbacher[1], **Kimberley N. White**[2], **Indranil Sen**[2], **Allen G. Oliver**[2], **Joseph P. Konopelski**[2], **Bridgette A. Barry**[1], and **Ólöf Einarsdóttir**[2]

[1]Department of Chemistry and Biochemistry and the Petit Institute for Bioengineering and Bioscience, Georgia Institute of Technology, Atlanta, Georgia 30332 USA

[2]Department of Chemistry and Biochemistry, University of California Santa Cruz, California 95064 USA

Abstract

Heme-copper oxidases have a crucial role in energy transduction mechanism, catalyzing the reduction of dioxygen to water. The reduction of dioxygen takes place at the binuclear center, which contains heme a_3 and Cu_B. The X-ray crystal structures have revealed that the C6' of tyrosine 244 (bovine heart numbering) is cross-linked to a nitrogen of histidine 240, a ligand to Cu_B. The role of the cross-linked tyrosine at the active site still remains unclear. In order to provide insight into the function of the cross-linked tyrosine, we have investigated the spectroscopic and electrochemical properties of chemical analogs of the Cu_B-His-Tyr site. The analogs, a tridentate histidine-phenol cross-linked ether ligand and the corresponding Cu-containing complex, were previously synthesized in our laboratory (White K. et al.; *Chem. Commun*. 3252–3254, 2007). Spectrophotometric titrations of the ligand and the Cu-complex indicate a pK_A of the phenolic proton of 8.8 and 7.7, respectively. These results are consistent with the cross-linked tyrosine playing a proton delivery role at the cytochrome oxidase active site. The presence of the phenoxyl radical was investigated at low temperature using electron paramagnetic resonance (EPR) and Fourier transform infrared (FT-IR) difference spectroscopy. UV-photolysis of the ligand, without bound copper, generated a narrow g = 2.0047 signal, attributed to the phenoxyl radial. EPR spectra recorded before and after UV photolysis of the Cu-complex showed a g = 2 signal characteristic of oxidized copper, suggesting that the copper is not spin-coupled to the phenoxyl radical. An EPR signal from the phenoxyl radical was not observed in the Cu-complex, either due to spin relaxation of the two unpaired electrons or to masking of the narrow phenoxyl radical signal by the strong copper contribution. Stable isotope (^{13}C) labeling of the phenol ring (C1') Cu-complex, combined with photo-induced difference FT-IR-spectroscopy, revealed bands at 1485 and 1483 cm^{-1} in the ^{12}C-minus-^{13}C isotope-edited spectra of the ligand and Cu-complex, respectively. These bands are attributed to the radical $\nu_{7a'}$ stretching frequency and are shifted to 1468 and 1472 cm^{-1}, respectively, with $^{13}C1'$ labeling. These results show that a radical is generated in both the ligand and the Cu-complex and support the unambiguous assignment of a vibrational band to the phenoxyl radical $\nu_{7a'}$ stretching mode. These data are discussed with respect to a possible role of the cross-linked tyrosine radical in cytochrome oxidase.

Correspondence to: Ólöf Einarsdóttir.

Supporting Information Available:
Synthetic protocols and ^1H NMR and ^{13}C NMR parameters for all compounds leading to the desired products; Figure S1: FT-IR absorbance spectra of tyrosinate (A), the natural abundance ligand (B), the ^{13}C ligand (C), the natural abundance Cu-complex (D), and the ^{13}C Cu-complex. Crystallographic data are available on request in CIF format as electronic supplementary information or from the Cambridge Crystallographic database.

Cytochrome *c* oxidase (C*c*O), the terminal enzyme in the respiratory electron transfer chain, plays a crucial role in energy transduction through the catalytic reduction of molecular oxygen to water.[1] This reaction drives the translocation of four protons across the inner mitochondrial or bacterial plasma membrane and generates the electrochemical proton gradient necessary for ATP synthesis.[2] The reduction of O_2 to water takes place at the heme *a3*/Cu_B binuclear site while avoiding the release of harmful, reactive oxygen species. The enzyme contains two additional redox centers, heme *a* and Cu_a. X-ray crystallographic studies on a variety of C*c*O enzymes[3–5] and protein chemical analysis[6] have identified a unique covalent cross-link between C6' of tyrosine 244 (bovine heart numbering) and the ε-nitrogen of histidine 240, a ligand to Cu_B. Mutational studies have revealed that this highly conserved, modified tyrosine is required for C*c*O enzymatic activity, although its specific biological function is under debate.[7, 8]

In the catalytic mechanism of O_2 reduction, scission of the O-O bond forms a so-called **P** intermediate with the heme *a3* iron in an oxyferryl state ($Fe_{a3}^{4+}=O^{2-}$).[9–11] The heme a_3 iron and Cu_B donate three of the four electrons required for the bond breakage. Under mixed-valence conditions, in which heme a_3 and Cu_B are reduced and heme *a* and Cu_A are oxidized, the origin of the fourth electron is still unknown. It has been proposed that due to its local proximity to the active site and its terminal location in the proton K-channel, the cross-linked tyrosine may act as an electron[12–16] and proton donor to O_2.[10, 17, 18]

Several infrared (IR) spectroscopic studies of cytochrome *c* oxidase from *Rhodobacter sphaeroides*,[16] *Paracoccus denitrificans*19–22 and bovine heart[19, 23, 24] have been carried out, but definitive assignment of spectral contributions from the tyrosine-histidine radical has been problematic. A previous EPR study on C*c*O incubated with H_2O_2[25] attributed a $g = 2$ signal to the cross-linked tyrosine. However, subsequent work showed that this signal may arise from a tryptophan cation radical[26–29] or another, unmodified tyrosyl radical.[13, 30, 31] Budiman et al. have proposed a radical migration pathway[30] from the cross-linked tyrosine radical to tyrosine 129 (bovine heart numbering).

These results suggest that the cross-linked tyrosine may play a role in O_2 reduction to water. To define its functional significance, several groups have synthesized and studied model compounds, which mimic the tyrosine-histidine cross-link[32–39] or the heme a_3/Cu_B binuclear site.[40–45] In a recent study, a functional C*c*O model was used to support the idea that the cross-linked tyrosine is essential for the catalytic reduction of O_2 under steady-state conditions.[46] Although these studies have afforded a better understanding of some of the physicochemical properties of the cross-link, little is known about the electronic structure of the Cu-coordinated tyrosine-histidine moiety.

Nagano and coworkers were the first to present vibrational assignments for a light-induced phenoxyl radical of a tyrosine-histidine-Cu_B model complex using resonance Raman spectroscopy.[38, 47] Recently, we reported the synthesis and structural characterization of two analogs of the active site of cytochrome *c* oxidase, a tridentate cross-linked histidine-phenol ligand and its corresponding Cu-complex.[39] Using spectrophotometric titrations, we showed that the acidity of the phenolic proton of the ligand is lower when compared to *p*-cresol. Subsequent Cu-coordination produced an additional decrease in pK_a, which is consistent with the proposed proton delivery role of the cross-linked tyrosine. In contrast to the ligand, the phenoxyl radical was not detected in the time-resolved optical absorption spectra recorded at room temperature of the copper-containing compound.[39]

In this study, we use stable isotopes to show that a phenoxyl radical is generated in a copper-containing histidine-phenol cross-linked model compound and assign vibrational bands to the radical and singlet forms.

Materials and Methods

Materials

L-Tyrosine, Tris(hydroxymethyl)aminomethane hydrochloride, acetonitrile, sodium hydroxide, and hydrochloric acid were purchased from Sigma (St. Louis, MO). $^{13}C_{4'}$-Tyrosine (98 – 99 %) was obtained from Cambridge Isotope Laboratories (Andover, MA).

Synthesis

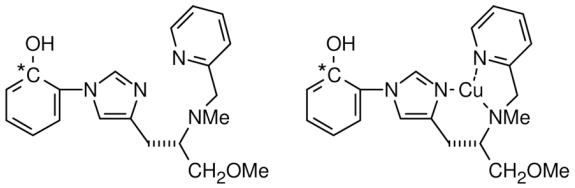

1 * = natural abundance
3 * = ^{13}C enriched

2 * = natural abundance
4 * = ^{13}C enriched

Synthesis of the unlabeled ligand **1** and copper complex **2** have already been described.[39] Whereas our previous synthesis relied on commercial 2-bromophenol as the starting material, preparation of the ^{13}C-labeled ligand **3** necessitated the use of 1-^{13}C-phenol (99% ^{13}C) as the starting material and required development of an alternative route to the key aryllead(IV) reagent.

Phenol in the presence of bromine and acetic acid yields, not unexpectedly, predominantly *p*-brominated material. Consequently, our attention was turned to directed ortho-metalation (DoM)[48] for specific C-2 activation. Considerable precedent exists in the literature for utilizing MOM protection as a directing group for *o*-metalation of phenolic compounds.[49, 50] Protection of the ^{13}C-phenol to provide **5** proceeded smoothly. However, extensive experimentation was necessary to identify a sufficiently selective and efficient method for the *o*-metalation. Success was achieved with *t*-BuLi in Et_2O at low temperature to yield trimethylstannane derivative **6** in 85% yield. Transmetalation of **6** afforded the desired aryllead(IV) reagent **7** (see Supporting Information for details).

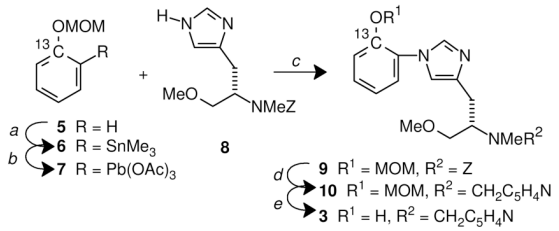

a) *t*-BuLi, $ClSnMe_3$, -25 °C, 90%; *b*) $Pb(OAc)_4$, cat. $Hg(O_2CCF_3)_2$, 86%;
c) cat. $Cu(OAc)_2$, 68%; *d*) 1) cyclohexadiene, Pd/C, 99%,
2) picolyl carboxaldehyde, $Na(OAc)_3BH$, 66%; *e*) $HCl_{(g)}$, then NaOH, 83%

The synthesis of the ^{13}C-labeled ligand **3** proceeded in an identical fashion to the synthesis of the non-labeled ligand **1**.[39] Aryllead reagent **7** was coupled to previously synthesized Z-protected *N*-methyl histidinol methyl ether (**8**) to afford **9**. Removal of the Cbz protection group and reductive amination installed the pyridine residue, yielding **10**. Finally, MOM-deprotection gave the ^{13}C-labeled ligand **3** in an overall yield of 29% from **5**. Addition of copper to ligand **3** under identical conditions as for the non-labeled ligand **1**[39] afforded a dark blue solution that yielded needles (**4**) suitable for single crystal X-ray analysis and biophysical studies. The ^{12}C-ligand (**1**) and the Cu-complex (**2**) will hereafter be referred to as the "ligand" and the "Cu-

complex;" the corresponding isotopically labeled compounds will be referred to as the ^{13}C-labeled ligand and Cu-complex.

Spectrophotometric Titrations

The pK_a values of the ^{13}C-labeled ligand and the corresponding Cu-complex were determined from the UV-visible spectra recorded on a Hewlett-Packard (8452) diode array spectrophotometer over the pH ranges 3.3–9.2 and 4.9–8.7, respectively. The values were compared to those obtained for the corresponding unlabeled compounds.[39] Due to limited solubility, the ^{13}C-labeled ligand and the Cu-complex were dissolved in 80% aqueous/20% acetonitrile mixtures in the presence of 0.1 M KCl. The spectra were analyzed by singular value decomposition (SVD) and global pK_a fitting as previously described[34] to determine the pK_a values and the intermediate spectra.

Electrochemical Titrations

Electrochemical experiments were carried out with a CH Instrument 440 electrochemical workstation at room temperature using a glassy carbon working electrode, Ag/AgCl (saturated with 0.1 M KCl) reference electrode and a platinum wire counter electrode.[51] The experiments were carried out in the presence of 10 mM Na-phosphate, pH 7.0 (0.2 M KCl).

EPR Spectroscopy

EPR spectra on samples in fused quartz sample tubes were recorded at 100 K on a Bruker (Billerica, MA) EMX 6/1 X-band EPR spectrometer, equipped with a ST-9605 cavity and a Wilmad (Buena, NJ) liquid nitrogen dewar.[34, 52] The unlabeled ligand and Cu-complex were prepared as 50 mM solutions in 35% acetonitrile/65% 10 mM Tris-HCl, pH 8.5 (ligand) or in 20% acetonitrile/80% 10 mM Tris-HCl, pH 6.2 (Cu-complex). Tyrosinate samples (50 mM) were prepared in 10 mM Tris-HCl, pH 11.0. The Cu-complex was unstable at high pH values, and limited solubility precluded the examination of 50 mM tyrosine and ligand solutions at pH 6.2. These high concentrations were necessary for comparison to the FT-IR experiments.

Tyrosyl or phenoxyl radicals were generated by photolysis with the 266 nm output from a Surelite III Nd:YAG laser (Continuum, Santa Clara, CA). The pulse energy was 70 – 80 mJ at a frequency of 10 Hz, and 50 flashes were employed. The spectrometer conditions were as follows: microwave frequency, 9.21 GHz; microwave power, 200 microW; modulation frequency, 100 kHz; modulation amplitude, 3 G; time constant, 2.6 s; conversion time, 1.3 s. Microwave power dependence experiments showed that there was no saturation of the signals from any of the samples under these conditions. The final photolysis-induced EPR spectrum was generated by subtracting background signals observed before photolysis using the Igor Pro v. 5.03 (Wavemetrics, Lake Oswego, OR) software.

FT-IR Spectroscopy

FT-IR spectra were obtained with a Nicolet Magna 550 II spectrometer, equipped with an MCT-A detector (Nicolet, Madison, WI). Samples were sandwiched between two CaF_2 windows, partitioned by a 6 μm spacer, and cooled to 79 K using a Hansen (R.G. Hansen & Associates, Santa Barbara, CA) liquid nitrogen cryostat prior to data collection. Sample conditions and preparations were similar to those described above for the EPR experiments, with the tyrosinate samples prepared at pH 11, and the ligand and Cu-complex at pH 8.5 and 6.2, respectively. Data were recorded before and after photolysis for 120 s at 4 cm^{-1} resolution and with a 2.5 cm s^{-1} mirror velocity. After two minutes of data collection, the samples were illuminated with 5 (tyrosinate and the ^{12}C and ^{13}C-labeled ligands) or 50 (^{12}C and ^{13}C-labeled Cu-complexes, buffer blank) 266 nm laser flashes using a Surelite III Nd:YAG laser (Continuum, Santa Clara, CA) with pulse energies of 70 – 80 mJ (at 10 Hz). The data were

processed using Omnic v. 5.2 software (Nicolet, Madison, WI), a Happ-Genzel apodization function, two levels of zero filling, and a Mertz phase correction. FT-IR absorption spectra and FT-IR light-minus-dark difference spectra were generated in Igor Pro v. 5.03 as previously described.[53] To construct the absorption spectrum, the single beam spectrum was ratioed to an open beam background, the absorbance was calculated, and the appropriate buffer blank interactively subtracted from the data.

Results

Structure of the Cu-complex

The structure of the ^{13}C-labeled Cu-tridentate ether complex was determined by single crystal X-ray analysis (Figure 1). As mentioned above, an alternative route toward synthesizing the aryllead(IV) reagent had to be developed because of the necessity to use different starting materials for the ^{12}C complex (2, bromophenol) and the ^{13}C-labeled ligand (1-^{13}C-phenol). There are four molecules of the complex and associated perchlorate anion in the unit cell of the primitive, acentric, orthorhombic space group $P2_12_12_1$ (see Supporting Information for details). The copper atom is coordinated in a square-planar geometry by three nitrogens of the ligand and a chlorine atom. The equatorial chloride forms a weak bond to copper in the adjacent monomeric unit (Cu-Cl: 2.76 Å). An analysis of the bond distances and angles about the C1', which was substituted with ^{13}C, reveals that the structure is within experimental error identical to our previously characterized ^{12}C-analogue.[39] The very slight variations observed in the derived parameters (bond distances and angles) are due to statistical variation (Table 1).

Spectrophotometric titrations

SVD and global pK_a fitting of the UV-visible spectra recorded for the ^{13}C-labeled ligand over a wide pH range revealed three pK_a values, 4.5, 7.4, and 8.8, which are attributed to the pyridine, imidazole, and phenol, respectively. These are identical within experimental error to our previously observed pK_a values for the unlabeled ligand.[39] A single pK_a of 7.7 was observed for the ^{13}C-labeled Cu-complex, which is consistent with a pK_a of 7.8 observed for the ^{12}C-analogue.[39]

Electrochemical Titrations

Cyclic voltammetry studies were performed on tyrosine, the natural abundance ligand, and the Cu-complex to access the effect of the cross-link and Cu^{2+} on the redox properties of the phenolate/phenoxyl radical couple. Figure 2A, 2B and 2C shows the cyclic voltammograms for the tyrosine, ligand, and Cu-complex, respectively. The cyclic voltammetry showed irreversible behavior, with anodic redox potentials of 0.67, 0.78 and 0.73 eV, respectively (950, 1060 and 1010 mV versus NHE electrode), attributed to the oxidation of tyrosine or phenol to the corresponding radicals in tyrosine, the ligand and the Cu-complex, respectively. A reversible peak with a redox potential of 0.42 eV in the Cu-complex is assigned to the Cu(II)/Cu(I) couple; this peak is absent in the ligand.

EPR Spectra

Figure 3 depicts the photolysis-induced EPR spectra (after photolysis-minus-before photolysis) derived from the natural abundance Cu-complex (panel A), ligand (panel B), and tyrosinate (panel C). For comparison, a photolysis-induced blank, acquired on the 35% acetonitrile/65% 10 mM Tris-HCl, pH 8.5, buffer alone is shown in Figure 3D. Figure 4 exhibits the EPR spectra of the ligand (panel A) and tyrosinate (panel B) on an expanded scale, displaying spectral line shapes. The UV photolysis of tyrosinate at 100 K generated an EPR signal (Figure 3C and Figure 4B) similar to the previously reported spectra,[54, 55] with a *g*-value of 2.0044. A previous EPR study of tyrosinate demonstrated that upon oxidation, the spin density is located on the

phenoxyl oxygen and carbons 1', 3', and 5' on the phenoxyl ring.[54] In the tyrosyl radical, the spectrum is dominated by hyperfine couplings to the C1' and C3' hydrogens, as well as conformation-sensitive couplings to the beta-methylene hydrogens.[54] At 1 mM concentrations, tyrosyl radicals exhibited a similar EPR lineshape at pH 5 and 11, although the signal intensity at pH 5 was ~50% of the amplitude observed at pH 11.[56] In the previous work, the change in signal intensity was attributed to the increase in midpoint potential of tyrosine at low pH values.

Photolysis of the ligand also generated a stable EPR signal (Figure 4A) with a similar *g*-value (2.0047) to the neutral tyrosyl radical.[52] The EPR spectrum of the ligand is similar to the spectrum we previously reported for a related His-phenol cross-linked compound.[34] Therefore, the EPR signal of the ligand suggests the formation of a neutral phenoxyl radical. The EPR line shape of the ligand (Figure 4A) lacks the hyperfine structure present in the tyrosinate spectrum (Figure 4B) due to the absence of beta-methylene protons. Moreover, spin quantization under non-saturating conditions showed that the radical yield is a factor of ~4 lower in the ligand, compared to tyrosinate.

Note that our EPR results differ from previous reports in which cross-linked compounds are based on *p*-cresol and in which hyperfine couplings to the equivalent -CH_3 protons dominate the EPR spectrum.[33, 36, 47] In earlier work, including our EPR simulations of the His-phenol cross-linked radical signal, it was concluded that the spin distribution on the phenoxyl radical is only modestly perturbed by the imidazole cross-link.[34, 36, 57] However, our previous time-resolved optical absorption spectra of the ligand[39] and the related cross-linked His-phenol compound[34] have shown that the imidazole crosslink causes a substantial red shift of the radical's electronic spectrum.

In the Cu-complex, an intense EPR signal from Cu^{2+} was observed both before and after photolysis (Figure 5), indicating that the oxidation state of the metal ion does not change. Photolysis was associated with only a small change in the amplitude of this copper signal (Figure 5, solid line, repeated from Figure 3), which is due to a background artifact created during subtraction of the spectra. A small baseline artifact was also apparent when experiments were conducted at lower Cu-complex concentrations, at which the expected copper hyperfine splittings could be observed (data not shown). The observation of a Cu^{2+} EPR signal after photolysis (Figure 5) indicates either that the resulting phenoxyl radical is not spin-coupled to the metal ion or that the phenoxyl radical produced by photolysis of the Cu-complex remains somehow undetectable by EPR. Our analysis of the FT-IR intensities (see below) suggests that the radical yield in the copper complex decreases by a factor of 40. This is supported by our time-resolved optical spectrum of the Cu-complex, which failed to show a 480–500 nm peak, attributed to the phenoxyl radical in analogous spectra of the ligand[39] and the related cross-linked His-phenol compound.[34] Nagano et al. [38] also did not did not observe a distinct band in the transient optical spectrum of their Cu-bound *ortho*-imidazole-bound *para*-cresol-based model compound.

FT-IR Spectroscopy

Photolysis-induced difference FT-IR spectroscopy was employed to monitor structural changes induced by oxidation. The FT-IR absorption spectra for tyrosinate and the ^{12}C and ^{13}C-labeled ligands and Cu-complexes were recorded (see Figure S1 in the Supporting Information). The FT-IR data were acquired before and after UV photolysis and then subtracted to generate the difference FT-IR spectra shown in Figure 6. Under the conditions employed in our FT-IR measurements, the phenol ring is expected to be unprotonated in tyrosinate (pK_A 10), primarily protonated (~67%) in the ligands (pK_A 8.9) and protonated in the Cu-complexes (pK_A 7.7–7.8). The limited solubility of tyrosine and the ligand at the high concentrations, necessary for FT-IR experiments, and the limited stability of the copper complex precluded the use of the same pH for all the experiments. Tyrosyl radical formation is expected to perturb

vibrational bands of the phenol ring (ν_{8a} and ν_{19a}) as well as the frequency of the CO vibrational band (ν7a').[58, 59] Negative bands in the difference spectra arise from vibrational bands unique to the ground (singlet) state of tyrosinate/phenol, whereas positive bands correspond to vibrational bands of the neutral tyrosyl/phenoxyl radical species. Only vibrational bands, which are perturbed by the oxidation of the phenol ring, will contribute to the photolysis-induced difference spectrum. As expected, photolysis of the blank (Figure 6A) resulted in no defined difference spectrum.

Ring and CO Stretching Vibrations of Tyrosinate/Phenol

In Figure 6B, negative bands of tyrosinate, corresponding to bands perturbed in the singlet state, are observed at 1605 (ν_{8a},), 1500 (ν_{19a}) and 1263 ($\nu_{7a'}$) cm^{-1}. These vibrational assignments are based upon previous reports.[52, 53, 60, 61] The assignments of other vibrational bands have been discussed.[34, 52, 61] A similar set of bands, with different frequencies, are observed for the ^{12}C-ligand (Figure 6C) and Cu-complex (Figure 6E). To assign these bands to ring and CO stretching frequencies, ^{13}C labeling of the CO ring carbon was performed in tyrosinate (C4'), the ligand (C1') (Figure 6D), and the Cu-complex (C1') (Figure 6F). All three vibrational bands, ν_{8a}, ν_{19a}, and $\nu_{7a'}$, are predicted to be sensitive to labeling at this ring position.[61] Isotope-edited spectra (double difference spectra), ^{12}C (light – dark)-minus-^{13}C (light – dark) were constructed to identify the frequencies of these isotope sensitive bands (Figure 7). In the isotope-edited spectra, the singlet bands from the ^{12}C-compound are negative; the ^{13}C-isotope shifted bands are positive. These bands are marked in Figure 7 with dotted lines.

As expected based on previous work,[52, 61] three negative bands in the tyrosinate isotope-edited spectrum (Figure 7A) at 1609 (ν_{8a}), 1501 (ν_{19a}), and 1268 ($\nu_{7a'}$) cm^{-1} show isotope shifts to 1600, 1490, and 1235 cm^{-1}, respectively (Table 2). These results are in reasonable agreement with the ^{13}C-isotope shifts predicted for these vibrational bands from DFT calculations.[61]

Isotope editing was also used to identify the analogous bands in the difference FT-IR spectra of the ligand and Cu-complex. From the isotope-edited spectrum of the ligand (Figure 7B), the negative bands at 1601, 1526, and 1292 cm^{-1} are attributed to ν_{8a}, ν_{19a} and $\nu_{7a'}$, respectively, with ^{13}C-isotope shifts (positive bands) to 1591, 1516, and 1276 cm^{-1}, respectively (Table 2 and Figure 7B). Our related, His-phenol cross-linked compound exhibited negative features at 1592, 1511, and 1265 cm^{-1}, which were assigned to perturbation of the singlet ν_{8a}, ν_{19a}, and $\nu_{7a'}$ bands, respectively, in the photolysis-induced FT-IR spectrum.[34] In the isotope-edited spectrum of the ^{12}C Cu-complex (Figure 7C), these same three vibrational modes appear at 1616, 1535, and 1234 cm^{-1}, with similar isotope shifts as those observed in the ligand (Table 2).

For the ligand in the singlet state, histidine-phenol cross-linking downshifts the highest energy, ν_{8a} phenol ring stretching mode and upshifts the ν_{19a} ring stretching mode (Table 2). Copper complexation upshifts both ring stretching modes relative to the non-metal-bound compound. Previously, changes in the frequency of the $\nu_{7a'}$ CO mode have been reported as a function of hydrogen bonding and protonation state of the phenol ring.[60] For a protonated phenol, the CO stretching vibration is observed between 1275 and 1265 cm^{-1} in proton donating states, with less intensity and at lower frequency (1240 and 1230 cm^{-1}) in proton accepting states, and at ~1255 cm^{-1} in non-hydrogen bonded states. For a deprotonated phenol, the CO vibrational band was reported at 1266 cm^{-1}. As mentioned above, under the conditions employed in our FT-IR measurements, the phenol ring is expected to be unprotonated in tyrosinate, protonated (67%) in the ligand and protonated in the Cu-complex. The upshift in CO frequency for the ligand (1292 cm^{-1}) compared to that of tyrosine (1268 cm^{-1}) is therefore larger than expected based on the expected change in protonation. The upshift is attributed to a strengthening of the C-O bond due to contribution of the C-C stretch to the 7a' mode in the cross-linked ligand. For an ortho-substituted amino phenol in a solid, a mode at 1290 cm^{-1} is predicted.[62]

In the ^{12}C-minus-^{13}C isotope edited spectra, the decrease in the CO frequency and intensity of the $\nu_{7a'}$ mode of the Cu-complex (1234 cm^{-1}) (Figure 7C), compared to the ligand (1292 cm^{-1}) (Figure 7B), is attributable to the expected change in protonation, if the COH group of the Cu-complex is hydrogen bonded as a proton acceptor. The origin of the derivative-shaped band at 1303/1292 cm^{-1} and the positive band at 1255 cm^{-1} in the Cu-complex (Figure 7C) is under investigation, but the observation of multiple ^{13}C-sensitive bands in this region suggests some heterogeneity in the CO frequency, and possibly, in the interactions of the phenolic OH group with the Cu^{2+} ion in the Cu-complex. An alternant pairing of the negative 1234 cm^{-1} band with the positive 1255 cm^{-1} band is considered less likely, due to the expectation that ^{13}C labeling will downshift the band,[61] and that the negative 1234 cm^{-1} band arises from the singlet state.

Ring and CO Stretching Vibrations of the Radical

Unique vibrational bands arising from the radical are observed as positive bands in the photo-induced difference spectra in Figure 6. In the ^{12}C-minus-^{13}C isotope-edited spectra (Figure 7), the natural abundance bands from the radical are positive (*) and the ^{13}C-shifted bands are negative (♦). The positive band at ~1517 cm^{-1} for tyrosine (Figure 7A, *) is assigned to the tyrosyl radical $\nu_{7a'}$ CO stretching band on the basis of multiple isotopic labeling experiments and DFT calculations.[52, 61] The frequency of the ^{13}C4'-shifted band is not obvious in the isotope-edited spectrum (Figure 7A) and may overlap with the negative ν_{19a} vibrational band at 1501 cm^{-1}. A ^{13}C-isotope shift of 27 cm^{-1} is predicted (Table 2).[61]

Based on the isotope-edited spectra (Figure 7B and 7C, *), the bands at 1485 and 1483, cm^{-1} , are attributed to the $\nu_{7a'}$ CO stretching in the ligand and Cu-complex, respectively. These bands shift to 1468 and 1472 cm^{-1} with ^{13}C labeling (Figure 7B and 7C, ♦; Table 2). The isotope-edited spectra in Figure 7 provide unambiguous support for the conclusion that a radical is generated by photolysis in both the ligand and the copper complex. In turn, this result confirms that the failure to observe a free radical signal in the EPR experiment is most likely due to the large background signal from the Cu^{2+} ion and/or the low photolysis yield of the radical.

The $\nu_{7a'}$ CO frequency is substantially downshifted in the ligand radical (Figure 7B) compared to the frequency observed in the tyrosyl radical (Figure 7A). Because the imidazole cross-linking does not significantly change the unpaired spin density distribution,[34] this effect may be caused by a decrease in the paired π-electron density in the CO bond or an inductive effect on the ionic character of the CO bond. However, the CO frequency in the radical state is not significantly shifted by copper (Figure 7B and 7C), suggesting that the CO frequency shifts observed in the radical states of the ligand and Cu-complex are not mediated by the partial negative charge on the phenolic oxygen.

In our previous studies on the related, histidine-phenol cross-linked compound, we suggested that the radical CO stretching vibration might arise from bands at 1522 or 1498 cm^{-1}.[34] However, ^{13}C-isotope-sensitive bands with these frequencies are not observed in the data presented here for the ligand or the Cu-complex. Assignment of a 1487 cm^{-1} band, observed previously in our histidine-phenol cross-linked compound,[34] to the CO stretching vibration is consistent with the data presented here.

Yield of the radical in the ligand and copper complex

To estimate the yield of the radical, the amplitudes of bands in the isotope-edited spectra (Figure 7) were compared after correction for any differences in concentration, flash number, flash energy, and gain. Our EPR measurements (Figure 4) suggest that the radical yield is decreased by a factor of 4, when tyrosinate is compared to the ligand. The FT-IR data in Figure 7A

(tyrosinate) and Figure 7B (ligand) were collected on different FT-IR spectrometers. However, analysis of the intensities of the CO $\nu_{7a'}$ band in Figure 7A (tyrosinate, 1268/1235 cm^{-1}) and B (ligand, 1292/1276 cm^{-1}) is qualitatively consistent with the EPR measurement. The FT-IR comparison predicts a 2.5 fold decrease in the ligand radical yield compared to tyrosine. A similar comparison was conducted for Figure 7B (ligand) and Figure 7C (copper complex), which were collected on the same FT-IR spectrometer, but with a different number of flashes (5, Figure 7B and 50, Figure 7C). Analysis of the intensities of the CO $\nu_{7a'}$ band in Figure 7B (ligand, 1292/1276 cm^{-1}) and 7C (1234/1224 cm^{-1}) gives a 40 fold decrease in the copper complex radical yield compared to that of the ligand.

Other vibrational bands

The broad ~1650 and ~1620 cm^{-1} peaks in the tyrosinate difference spectrum (Figure 6B) have previously been assigned to an overlap of solvent bands and perturbed NH_2 bending modes.[52, 61, 63] The photo-induced difference spectra of the natural abundance and ^{13}C-labeled ligand and Cu-complexes (Figure 6C – 6F) contain a similar series of broad peaks in the ~1660 – 1650 cm^{-1} region. However, these compounds do not contain any NH bands that can be perturbed upon oxidation. Therefore, in the case of the ligand and the Cu-complex, these broad bands are attributed to changes in solvent interactions alone.

The ν_{8a} ring stretching mode of the tyrosyl radical is expected between 1550–1560 cm^{-1}.[52, 59, 61] A candidate for this band is observed at 1554 cm^{-1} in the isotope-edited spectrum for tyrosinate (Figure 7A); however, the magnitude of the experimental isotope shift has not been established.[61] DFT calculations predict that the ν_{8a} ring stretching mode of the radical will be insensitive to ring 4' labeling.[61, 64] In agreement with this expectation, the ν_{8a} ring stretching mode is not observed in the isotope-edited spectra derived from the ligand and the Cu-complex (Figure 7B and 7C).

Some vibrational bands are observed in the ^{12}C and ^{13}C-labeled ligands and Cu-complexes but are absent in the tyrosinate difference spectrum (Figure 6). These bands may arise from a perturbation of the imidazole cross-link upon radical formation. One such band appears at 1511–1508 cm^{-1} (pos.)/1494–1490 cm^{-1} (neg.) in the ligands and Cu-complexes (Figure 6C–F). The analogous positive peak may be at 1522 cm^{-1} in our related phenol-histidine cross-linked model.[34]

Discussion

Spectrophotomotmetric titrations

Our previous spectrophotmetric titrations on the natural abundance ligand and its copper complex[39] and those presented here for the ^{13}C-labeled ligand and Cu-complex have measured the pK_a of the phenolic proton. These studies indicate that the ligand pK_a of 8.8 and the Cu-complex pK_a of 7.8 are significantly lower than the pK_a of tyrosine.[34] These results are consistent with the cross-linked tyrosine facilitating proton delivery at the enzyme active site. These data are in agreement with previous studies on other model compounds,[33, 37, 65] which gave a pK_a value of 8.65 for a tripodal chelating ligand, containing an *ortho*-imidazole-phenol linkage, and a pK_a of 8 for a corresponding Zn- complex. For the ligand, a lower phenolic pK_a compared to unperturbed tyrosine or phenol would be expected, either through an inductive electron-withdrawing effect or through resonance stabilization of the phenolate anion by the N-linked imidazole.[37, 43] Further reduction would be expected upon coordination of the cross-linked imidazole to the copper because copper will withdraw electron density from the imidazole and stabilize the phenolate anion.[65]

Electrochemical titrations

The 670 mV potential of tyrosine (950 mV vs NIH electrode) is similar to that reported previously at pH 7.0.[66] At pH 7.0, our electrochemical data indicate that the redox potentials of the ligand phenol and the Cu-complex phenol are 110 and 60 mV more positive than that of tyrosine, respectively, consistent with imidazole withdrawing electron density from the phenol ring.[33] The 110 mV increase in the redox potential of the ligand over that of tyrosine is similar to that observed previously between the oxidation potential of 2-imidazol-1-yl-4-methylphenol and *p*-cresol (66 mV) recorded at pH 11.5.[33] The lowering of the phenolic proton pK_A may ensure proton delivery during dioxygen reduction, and the moderate increase in the potential of the Cu-complex (60 mV) compared to that of unperturbed tyrosine may allow re-reduction of the tyrosyl radical following its oxidation during the splitting of the dioxygen bond.[33]

EPR

UV-photolysis of polycrystalline samples of the ligand clearly generated a paramagnetic species as indicated by a relatively narrow EPR signal with a corresponding isotropic *g*-value of 2.0047. This observed *g*-value is in good agreement with the *g*-value of the tyrosyl radical and suggests the formation of a neutral phenoxyl radical in the ligand. This result also suggests that the spin distribution of the photolysis-induced phenoxyl radical is not noticeably perturbed upon addition of an *o*-substituted imidazole group. Our previous EPR simulations on the related histidine-phenol cross-linked compound corroborate this idea.[34] DFT calculations have also shown that *o*-substitution yields only minor effects on the spin distribution of the deprotonated cross-linked tyrosine radical, consistent with our results.[57, 67] EPR studies of other tyrosine-histidine model compounds have confirmed this conclusion.[36]

Previously, it was proposed that the S = 1/2 tyrosyl radical in cytochrome *c* oxidase might spin couple with the S = 1/2 Cu_B.[10, 68] This would result in no Cu_B^{2+} EPR signal as observed for the magnetically-coupled Cu-tyrosyl radical in galactose oxidase.[69, 70] However, Collman and coworkers have shown that a tyrosyl radical near a binuclear site analog does not necessarily spin couple with Cu_B.[46] The absence of a phenoxyl radical EPR signal for the Cu-complex presented here is consistent with tyrosine-histidine-Cu_B model studies with[46] or without[47] a heme group. Nagano and coworkers[47] observed no EPR phenoxyl radical signal for a copper ligated 2-[4-[[bis(1-methyl-1H-imidazol-2ylmethyl)amino]methyl]-1H-imidazol-1-yl]-4methylphenol compound, Cu^{II}-**BIAIP**, upon light excitation in a temperature range from 4 to 90 K. This lack of a phenoxyl radical EPR signal was attributed to a weak signal intensity stemming from spin relaxation of the two unpaired interacting electrons.[47] From the relative intensities of the tyrosinate, ligand and Cu-complex EPR signals in our studies, it is evident that production of a phenoxyl radical species in the Cu-complex will be masked by the broad EPR signal from Cu^{2+} itself (Figure 3 and Figure 5). Thus conventional continuous-wave X-band EPR spectroscopy alone is too insensitive for the detection of such a paramagnetic species. The absence of a phenoxyl radical in our time-resolved optical absorption spectra generated following UV-photolysis of the Cu-complex was attributed to possibly quenching by the copper.[39]

A tyrosine radical has been identified in the $\mathbf{P_M}$ and the $\mathbf{F}\cdot$ oxyferryl intermediates of *P. denitrificans* using EPR spectroscopy;[30] these intermediates were generated upon addition of stoichiometric amounts of hydrogen peroxide to the oxidized enzyme at high and low pH, respectively. This radical has been assigned to tyrosine 129 (Tyr 167 *in P. denitrificans*) based on a multifrequency EPR (34 and 285 GHz) study of various tyrosine variants close to the binuclear center. However, because mutation of this tyrosine does not severely impact the turnover activity of the enzyme, it may not be involved in direct electron donation at the binuclear center during dioxygen turnover.[26, 30]

FT-IR spectroscopy

Photolysis-induced FT-IR difference spectra were acquired to gain structural information and provide insight into the functional role of the tyrosine-histidine moiety in C*c*O. FT-IR spectroscopy detects changes in force constants, which are associated with UV photolysis and phenoxyl radical generation. Unique positive vibrational modes were detected in the ligand and the Cu-complex compared to the tyrosyl radical, indicating that that the *o*-substituted imidazole force constants are perturbed upon oxidation of the phenoxyl group. This conclusion is supported by our previous FT-IR studies of a related cross-linked histidine-phenol analog[34] and by previous *ab initio* calculations[67] for histidine-substituted tyrosine models. We also observed a large spectral shift (~100 nm) in the time-resolved optical absorption difference spectra between the radical generated in the ligand and unperturbed tyrosyl radical,[39] which may suggest significant mixing of the imidazole and phenoxyl electronic states in the ligand.

Upon oxidation, the frequencies of the radicals in the ligand and the Cu-complex are essentially identical and thus the copper does not seem to dramatically alter the electronic structure of the radical species. This observation is consistent with resonance Raman data reported for the biomimetic cross-linked **BIAIP** ligand and Cu^{II}-**BIAIP** compound although the resonance Raman frequencies reported for the 7a' mode are significantly higher than those reported here.[47] Stable isotope labeling of the C1' carbon in the present study aided in the assignment of the CO frequency of the cross-linked phenoxyl radical in the ligand and the Cu-complex. Our assignments are consistent with FT-IR vibrational assignments for the tyrosine-histidine radical in cytochrome *c* oxidase. A band at 1489 cm^{-1} in the Raman spectrum of the $\mathbf{P_M}$ state of cytochrome bo_3 was tentatively assigned to the ν(CO) of the tyrosine-histidine radical.[71] In previous FT-IR difference studies, a frequency of 1479 cm^{-1} in the $\mathbf{P_M}$- minus-**O** spectrum of both the *R. sphaeroides*[16] and *P. denitrificans*[19] enzymes was attributed to the CO stretching vibration of the tyrosyl radical. Recently, based on isotope labeling, a band at 1519 cm^{-1} was identified as the phenoxyl radical ring stretching frequency of the cross-linked tyrosine in the $\mathbf{P_M}$-minus-**O** FT-IR difference spectrum of *P. denitrificans* C*c*O.[21] Nyquist and coworkers attributed bands at 1528 and 1517 cm^{-1} to the C-C ring stretching frequencies of the tyrosine-histidine radical in *R. sphaeroides* cytochrome *c* oxidase.[16] However, previous Raman spectroscopic studies of *ortho*-imidazole-bound *para*-cresol-based model compounds, with and without copper, have attributed bands around 1530 – 1533 cm^{-1} to the CO stretching vibration.[35, 38, 47] The good agreement between the vibrational assignments presented here for the ligand and the Cu-complex and those observed in the spectra of the $\mathbf{P_M}$ intermediate of cytochrome *c* oxidase from different species provides further support for the presence of a tyrosyl radical in the $\mathbf{P_M}$ intermediate of cytochrome oxidase. These data indicate that these compounds are useful markers for future assignments of additional, tyrosine-histidine crosslink vibrational bands in C*c*O.

Several experimental results argue against the FTIR bands resulting from a dissociated ligand in solution rather than the Cu-complex. First, the time-resolved optical absorption spectrum of the ligand shows a band at ~500 nm, while the spectrum of the Cu-complex does not. The spectrophotometric titrations of the ligand and the Cu-complex give significantly different pK_a values for the phenolic proton (8.8 for the ligand, and 7.7 for the Cu-complex); the additional pK_a values of 4.5 and 7.4, attributed to the pyridine and imidazole, are not observed in the Cu-complex, arguing against a dissociated ligand being present in the Cu-complex sample. A phenoxyl radical signal is observed in the EPR spectrum of the photoinduced ligand while this signal is absent in the Cu-complex. Moreover, while the vibrational frequencies attributed to the C–O stretch of the cross-linked phenoxyl radical are similar in the ligand and the Cu-complex, the C-O stretches for the phenolate anion in the two compounds are significantly different. Furthermore, we expect the Cu-imidazole bond to be stable at pH 6.2 and only at significantly lower pH, might the imidazole become protonated and the Cu-bond

break. A Jahn-Teller effect would be most prominent in the axial (dz^2) direction and not along the equatorial Cu-imidazole bond.

In summary, our studies show that a Cu^{2+} EPR signal is detected in the Cu complex both before and after photolysis. Stable isotope (^{13}C) labeling of the phenol ring provides unequivocal support for the formation of the phenoxyl radical in both the ligand and the Cu-complex, following UV photolysis. Moreover, our results indicate that the C-O stretching frequency of the cross-linked tyrosyl radical would be expected at ~1480–1490 cm^{-1} rather that in the 1530–1535 cm^{-1}. Together, our EPR and FT-IR results suggest that Cu_B^{2+} at the active site of cytochrome oxidase is not spin-coupled to the cross-linked tyrosyl radial. Collman and coworkers have shown that a stable Fe^{III}-superoxide-Cu^{I} CcO model compound reacts intermolecularly with exogeneous Tyr244 mimic compounds. This reaction leads to the formation of a phenoxyl radical and an oxyferryl ($Fe^{IV}=O^{2-}$)-cupric species, which is analogous to that observed in the **P** intermediate of the enzyme.[44] Moreover, mutagenesis of the cross-linked tyrosine to phenylalanine or histidine leads to essentially an inactive enzyme, reflecting the importance of this residue[7, 72] The absence of an EPR signal from the cross-linked tyrosyl radical in current EPR studies on cytochrome oxidase has been suggested to be due to the migration of the cross-linked tyrosine radical to tyrosine 129 (Tyr 167 in *P. denitrificans*).[13, 30] This pathway would compensate for the expected thermodynamic barrier to the fourth electron reduction reaction.[73] MacMillan et al. have suggested that tryptophan 126 (Trp 272 in *P. denitrificans*) may be an important intermediate on this pathway.[26] Our results demonstrate that the fourth electron required for dioxygen bond cleavage may indeed first originate on the cross-linked tyrosine, with the radical ultimately ending up on tyrosine 129 by the way of tryptophan 126.

Supplementary Material

Refer to Web version on PubMed Central for supplementary material.

Acknowledgment

This work was supported by the National Institutes of Health grant GM53788 (Ó.E), and GM 43273 (B.A.B). The single crystal X-ray diffraction data in this work were recorded on an instrument supported by the National Science Foundation, Major Research Instrumentation (MRI) Program under Grant No. CHE-0521569. We would like to thank Sulolit Pradhan and Shaowei Chen for assistance with the electrochemical measurements.

References

1. Ferguson-Miller S, Babcock GT. Heme/copper terminal oxidases. Chem. Rev 1996;96:2889–2907. [PubMed: 11848844]
2. Wikström MKF. Proton pump coupled to cytochrome *c* oxidase in mitochondrion. Nature 1977;266:271–273. [PubMed: 15223]
3. Yoshikawa S, Shinzawa-Itoh K, Nakashima R, Yanoe R, Yamashita E, Inoue N, Yao M, Fei MJ, Libeu CP, Mitzushima T, Yamaguchi H, Tomizaki T, Tsukihara T. Redox-coupled crystal structure changes in bovine heart cytochrome *c* oxidase. Science 1998;280:1723–1731. [PubMed: 9624044]
4. Ostermeier C, Harrenga A, Ermler U, Michel H. Structure at 2.7 Å resolution of the Paracoccus denitrificans two-subunit cytochrome *c* oxidase complexed with an antibody F_V fragment. Proc. Natl. Acad. Sci. U.S.A 1997;94:10547–10553. [PubMed: 9380672]
5. Soulimane T, Buse G, Bourenkov GP, Bartunik HD, Huber R, Than ME. Structure and mechanism of the aberrant ba_3-cytochrome *c* oxidase from Thermus thermophilus. EMBO J 2000;19:1766–1776. [PubMed: 10775261]
6. Buse G, Soulimane T, Dewor M, Meyer HE, Blüggel M. Evidence for a copper-coordinated histidine–tyrosine cross-link in the active site of cytochrome oxidase. Protein Science 1999;8:958–990. [PubMed: 10338006]

7. Das TK, Pecoraro C, Tomson FL, Gennis RB, Rousseau DL. The post-translational modification in cytochrome *c* oxidase is required to establish a functional environment of the catalytic site. Biochemistry 1998;37:14471–14476. [PubMed: 9772174]
8. Pinakoulaki E, Pfitzner U, Ludwig B, Varotsis C. The role of the cross-link His-Tyr in the functional properties of the binuclear center in cytochrome *c* oxidase. J. Biol. Chem 2002;277:13563–13568. [PubMed: 11825904]
9. Ogura T, Hirota S, Proshlyakov DA, Shinzawa-Itoh K, Yoshikawa S, Kitagawa T. Time-resolved resonance Raman evidence for tight coupling between electron transfer and proton pumping of cytochrome *c* oxidase upon the change from the Fe^{V} oxidation level to the Fe^{IV} oxidation level. J. Am. Chem. Soc 1996;118:5443–5449.
10. Proshlyakov DA, Pressler MA, Babcock GT. Dioxygen activation and bond cleavage by mixed-valence cytochrome *c* oxidase. Proc. Natl. Acad. Sci. U.S.A 1998;95:8020–8025. [PubMed: 9653133]
11. Fabian M, Wong WW, Gennis RB, Palmer G. Mass spectrometric determination of dioxygen bond splitting in the “peroxy” intermediate of cytochrome *c* oxidase. Proc. Natl. Acad. Sci. U.S.A 1999;96:13114–13117. [PubMed: 10557282]
12. Blomberg MRA, Siegbahn PEM, Babcock GT, Wikström MKF. O—O bond splitting mechanism in cytochrome oxidase. J. Inorg. Biochem 2000;80:261–269. [PubMed: 11001098]
13. Svistunenko DA, Wilson MT, Cooper CE. Tryptophan or tyrosine? On the nature of the amino acid radical formed following hydrogen peroxide treatment of cytochrome *c* oxidase. Biochim. Biophys. Acta 2004;1655:372–380. [PubMed: 15100053]
14. Proshlyakov DA, Pressler MA, DeMaso C, Leykam JF, Dewitt DL, Babcock GT. Oxygen activation and reduction in respiration: Involvement of redox-active tyrosine 244. Science 2000;290:1588–1591. [PubMed: 11090359]
15. Tomson F, Bailey JA, Gennis RB, Unkefer CJ, Li ZH, Silks LA, Martinez RA, Donohoe RJ, Dyer RB, Woodruff WH. Direct infrared detection of the covalently ring linked His-Tyr structure in the active site of the heme-copper oxidases. Biochemistry 2002;41:14383–14390. [PubMed: 12450405]
16. Nyquist RM, Heitbrink D, Bolwien C, Gennis RB, Heberle J. Direct observation of protonation reactions during the catalytic cycle of cytochrome *c* oxidase. Proc. Natl. Acad. Sci. U.S.A 2003;100:8715–8720. [PubMed: 12851460]
17. Gennis RB. Multiple proton-conducting pathways in cytochrome oxidase and a proposed role for the active-site tyrosine. Biochim. Biophys. Acta 1998;1365:241–248.
18. Sucheta A, Szundi I, Einarsdóttir Ó. Intermediates in the reaction of fully reduced cytochrome *c* oxidase with dioxygen. Biochemistry 1998;37:17905–17914. [PubMed: 9922158]
19. Iwaki M, Puustinen A, Wikström MKF, Rich PR. ATR-FTIR spectroscopy of the P_M and F intermediates of bovine and *Paracoccus denitrificans* cytochrome *c* oxidase. Biochemistry 2003;42:8809–8817. [PubMed: 12873142]
20. Iwaki M, Puustinen A, Wikström MKF, Rich PR. ATR-FTIR spectroscopy and isotope labeling of the P_M intermediate of *Paracoccus denitrificans* cytochrome *c* oxidase. Biochemistry 2004;43:14370–14378. [PubMed: 15533041]
21. Iwaki M, Puustinen A, Wikström MKF, Rich PR. Structural and chemical changes of the P_M intermediate of *Paracoccus denitrificans* cytochrome *c* oxidase revealed by IR spectroscopy with labeled tyrosines and histidine. Biochemistry 2006;45:10873–10885. [PubMed: 16953573]
22. Hellwig P, FPfitzner U, Behr J, Rost B, Pesavento RP, van der Donk WA, Gennis RB, Michel H, Ludwig B, Mäntele W. Vibrational modes of tyrosines in cytochrome *c* oxidase from *Paracoccus denitrificans*: FTIR and electrochemical studies on Tyr-D_4-labeled and on Tyr280His and Tyr35Phe mutant enzymes. Biochemistry 2002;41:9116–9125. [PubMed: 12119026]
23. Iwaki M, Breton J, Rich PR. ATR-FTIR difference spectroscopy of the P_M intermediate of bovine cytochrome *c* oxidase. Biochim. Biophys. Acta 2002;1555:116–121. [PubMed: 12206902]
24. Rich PR, Breton J. Attenuated total reflection Fourier transform infrared studies of redox changes in bovine cytochrome *c* oxidase: Resolution of the redox Fourier transform infrared difference spectrum of heme a_3. Biochemistry 2002;41:967–973. [PubMed: 11790120]

25. MacMillan F, Kannt A, Behr J, Prisner T, Michel H. Direct evidence for a tyrosine radical in the reaction of cytochrome *c* oxidase with hydrogen peroxide. Biochemistry 1999;38:9179–9184. [PubMed: 10413492]
26. MacMillan F, Budiman K, Angerer H, Michel H. The role of tryptophan 272 in the *Paracoccus denitrificans* cytochrome *c* oxidase. FEBS Lett 2006;580:1345–1349. [PubMed: 16460733]
27. Rich PR, Rigby SEJ, Heathcote P. Radicals associated with the catalytic intermediates of bovine cytochrome *c* oxidase. Biochim. Biophys. Acta 2002;1557:137–146. [PubMed: 12160986]
28. Rigby SEJ, Jünemann S, Rich PR, Heathcote P. Reaction of bovine cytochrome *c* oxidase with hydrogen peroxide produces a tryptophan cation radical and a porphyrin cation radical. Biochemistry 2000;39:5921–5928. [PubMed: 10821663]
29. Wiertz FG, Richter O-MH, Ludwig B, de Vries S. Kinetic resolution of a tryptophan-radical intermediate in the reaction cycle of *Paracoccus denitrificans* cytochrome *c* oxidase. J. Biol. Chem 2007;282:31580–31591. [PubMed: 17761680]
30. Budiman K, Kannt A, Lyubenova S, Richter OH, Ludwig B, Michel H, MacMillan F. Tyrosine 167: The origin of the radical species observed in the reaction of cytochrome *c* oxidase with hydrogen peroxide in *Paracoccus denitrificans*. Biochemistry 2004;43:11709–11716. [PubMed: 15362855]
31. Chen YR, Gunther RP, Mason RP. An electron spin resonance spin-trapping investigation of the free radicals formed by the reaction of mitochondrial cytochrome *c* oxidase with H_2O_2. J. Biol. Chem 1999;274:3308–3314. [PubMed: 9920871]
32. Elliott GI, Konopelski JP. Complete *N*-1 regiocontrol in the formation of *N*-arylimidazoles. Synthesis of the active site His-Tyr side chain coupled dipeptide of cytochrome *c* pxidase. Org. Lett 2000;2:3055–3057. [PubMed: 11009344]
33. McCauley KM, Vrtis JM, Dupont J, van der Donk WA. Insights into the functional role of the tyrosine-histidine linkage in cytochrome *c* oxidase. Org. Lett 2000;122:2403–2404.
34. Cappuccio JA, Ayala I, Elliott GI, Szundi I, Lewis J, Konopelski JP, Barry BA, Einarsdóttir Ó. Modeling the active site of cytochrome oxidase: Synthesis and characterization of a cross-linked histidine-phenol. J. Am. Chem. Soc 2002;124:1750–1760. [PubMed: 11853453]
35. Aki M, Ogura T, Naruta Y, Le TH, Sato T, Kitagawa T. UV resonance Raman characterization of model compounds of Tyr^{244} of bovine cytochrome *c* oxidase in its neutral, deprotonated anionic, and deprotonated neutral radical forms: Effects of covalent binding between tyrosine and histidine. J. Phys. Chem. A 2002;106:3436–3444.
36. Kim SH, Aznar C, Brynda M, Silks LA, Michalczyk R, Unkefer CJ, Woodruff WH, Britt RD. An EPR, ESEEM, structural NMR, and DFT study of a synthetic model for the covalently ring-linked tyrosine-histidine structure in the heme-copper oxidases. J. Am. Chem. Soc 2004;126:2328–2338. [PubMed: 14982436]
37. Pratt DA, Pesavento RP, van der Donk WA. Model studies of the histidine-tyrosine cross-link in cytochrome *c* oxidase reveal the flexible substituent effect of the imidazole moiety. Org. Lett 2005;7:2735–2738. [PubMed: 15957934]
38. Nagano Y, Liu J, Naruta Y, Kitagawa T. UV resonance Raman study of model complexes of the Cu_B site of cytochrome *c* oxidase. J. Mol. Struct 2005;735:279–291.
39. White KN, Sen I, Szundi I, Landaverry YR, Bria LE, Konopelski JP, Olmstead MM, Einarsdóttir Ó. Synthesis and structural characterization of cross-linked histidine-phenol Cu(II) complexes as cytochrome *c* oxidase active site models. Chem. Commun 2007:3252–3254.
40. Liu JG, Naruta Y, Tani F. A functional model of the cytochrome *c* oxidase active site: Unique conversion of a heme-μ-peroxo-Cu^{II} intermediate into heme- superoxo/Cu^{I}. Angew. Chemie Internatl. Edition 2005;44:1836–1840.
41. Liu JG, Naruta Y, Tani F, Chishiro T, Tachi Y. Formation and spectroscopic characterization of the dioxygen adduct of a heme-Cu complex possessing a cross-linked tyrosine-histidine mimic: modeling the active site of cytochrome *c* oxidase. Chem. Commun 2004;1:120–121.
42. Kamaraj K, Kim E, Galliker B, Zakharov LN, Rheingold AL, Zuberbühler AD, Karlin KD. Copper (I) and copper(II) complexes possessing cross-linked imidazole-phenol ligands: Structures and dioxygen reactivity. J. Am. Chem. Soc 2003;125:6028–6029. [PubMed: 12785812]

43. Kim E, Kamaraj K, Galliker B, Rubie ND, Moënne-Loccoz P, Kaderli S, Zuberbühler AD, Karlin KD. Dioxygen reactivity of copper and heme-copper complexes possessing an imidazole-phenol cross-link. Inorg. Chem 2005;44:1238–1247. [PubMed: 15732964]
44. Collman JP, Decréau RA, Sunderland CJ. Single-turnover intermolecular reaction between a Fe^{III}–superoxide–Cu^{I} cytochrome *c* oxidase model and exogeneous Tyr244 mimics. Chem. Commun 2006:3894–3896.
45. Collman JP, Decréau RA, Zhang C. Synthesis of cytochrome *c* oxidase models bearing a Tyr^{244} Mimic. J. Org. Chem 2004;69:3546–3549. [PubMed: 15132568]
46. Collman JP, Devaraj NK, Decréau RA, Yang Y, Yan YL, Ebina W, Eberspacher TA, Chidsey CED. A cytochrome *c* oxidase model catalyzes oxygen to water reduction under rate-limiting electron flux. Science 2007;315:1565–1568. [PubMed: 17363671]
47. Nagano Y, Liu J, Naruta Y, Ikoma T, Tero-Kubota S, Kitagawa T. Characterization of the phenoxyl radical in model complexes for the Cu_B site of cytochrome *c* oxidase: Steady-state and transient absorption measurements, UV resonance Raman spectroscopy, EPR spectroscopy, and DFT calculations for M-BIAIP. J. Am. Chem. Soc 2006;128:14560–14570. [PubMed: 17090040]
48. Snieckus V. Directed ortho metalation. Tertiary amide and O-carbamate directors in synthetic strategies for polysubstituted aromatics. Chem. Rev 1990;90:879–933.
49. Kaiser F, Schwink L, Velder J, Schmalz HG. Studies towards the total synthesis of mumbaistatin: synthesis of highly substituted benzophenone and anthraquinone building blocks. Tetrahedron 2003;59:3201–3217.
50. Seganish WM, DeShong P. Application of directed orthometalation toward the synthesis of aryl siloxanes. J. Org. Chem 2004;69:6790–6795. [PubMed: 15387604]
51. Deng F, Chen S. Electrochemical quartz crystal microbalance studies of the rectified quantized charging of gold nanoparticle multilayers. Langmuir 2007;23:936–941. [PubMed: 17209655]
52. Ayala I, Range K, York D, Barry BA. Spectroscopic properties of tyrosyl radicals in dipeptides. J. Am. Chem. Soc 2002;124:5496–5505. [PubMed: 11996592]
53. Vassiliev IR, Offenbacher AR, Barry BA. Redox-active tyrosine residues in pentapeptides. J. Phys. Chem. B 2005;109:23077–23085. [PubMed: 16854006]
54. Barry BA, El-Deeb MK, Sandusky PO, Babcock GT. Tyrosine radicals in photosystem II and related model compounds. Characterization by isotopic labeling and EPR spectroscopy. J. Biol. Chem 1990;256:20139–20143. [PubMed: 2173697]
55. Hulsebosch RJ, van den Brink JS, Nieuwenhuis AM, Gast P, Rapp J, Lugtenburg J, Hoff AJ. Electronic structure of the neutral tyrosine radical in frozen solution. Selective ^{2}H-, ^{13}C-, and ^{17}O-isotope labeling and EPR spectroscopy at 9 and 35 GHz. J. Am. Chem. Soc 1997;119:8685–8694.
56. Sibert R, Josowicz M, Porcelli F, Veglia G, Range K, Barry BA. Proton-coupled electron transfer in a biomimetic peptide as a model of enzyme regulatory mechanisms. J. Am. Chem. Soc 2007;129:4393–4400. [PubMed: 17362010]
57. Himo F, Erikson LA, Blomberg MRA, Siegbahn PEM. Substituent effects on OH bond strength and hyperfine properties of phenol as model for modified tyrosyl radicals in proteins. Internatl. J. Quant. Chem 2000;76:714–723.
58. Tripathi GNR, Schuler RH. The resonance Raman spectrum of phenoxyl radical. J. Chem. Phys 1984;81:113–121.
59. Johnson CR, Ludwig M, Asher SA. Ultraviolet resonance Raman characterization of photochemical transients of phenol, tyrosine, and tryptophan. J. Am. Chem. Soc 1986;108:905–912.
60. Takeuchi H, Watanabe N, Satoh Y, Harada I. Effects of hydrogen bonding on the tyrosine Raman bands in the 1300-1150 cm^{-1} region. J. Raman Spectr 1989;20:233–237.
61. Range K, Ayala I, York D, Barry BA. Normal modes of redox-active tyrosine: conformation dependence and comparison to experiment. J. Phys. Chem. B 2006;110:10970–10981. [PubMed: 16771350]
62. Agashe MS, Jose CI. Analysis of complex hydroxyl absorptions of amino- and dimethylamino-phenols. J. Chem. Soc., Faraday Transact. 2: Mol. and Chem. Physics 1976;73:1227–1231.
63. McCracken J, Vassiliev IR, Yang EC, Range K, Barry BA. ESEEM studies of peptide nitrogen hyperfine coupling in tyrosyl radicals and model peptides. J. Phys. Chem. B 2007;111:6586–6592. [PubMed: 17518496]

64. McDonald W, Einarsdóttir Ó. Solvent effects on the vibrational frequencies of phenolate anion, para-cresolate anion and their radicals. J. Phys. Chem. A 2008;112:11400–11413. [PubMed: 18939813]

65. Pesavento RP, Pratt DA, Jeffers J, van der Donk WA. Model studies of the Cu_B site of cytochrome *c* oxidase utilizing a Zn(II) complex containing an imidazole–phenol cross-linked ligand. Dalton Transact 2006;27:3326–3337.

66. Harriman A. Further comments on the redox potentials of tryptophan and tyrosine. J. Phys. Chem 1987;91:6102–6104.

67. Bu Y, Cukier RI. Structural character and energetics of tyrosyl radical formation by electron/proton transfers of a covalently linked histidine-tyrosine: A model for cytochrome *c* oxidase. J. Phys. Chem. B 2005;109:22013–22026. [PubMed: 16853859]

68. Palmer G. Current issues in the chemistry of cytochrome *c* oxidase. J. Bioenerg. Biomembr 1993;25:145–153. [PubMed: 8389747]

69. Whittaker MM, Whittaker JW. A tyrosine-derived free radical in apogalactose oxidase. J. Biol. Chem 1990;265:9610–9613. [PubMed: 2161837]

70. Whittaker MM, Whittaker JW. The active site of galactose oxidase. J. Biol. Chem 1988;263:6074–6080. [PubMed: 2834363]

71. Uchida T, Mogi T, Kitagawa T. Resonance Raman studies of oxo intermediates in the reaction of pulsed cytochrome *bo* with hydrogen peroxide. Biochemistry 2000;39:6669–6678. [PubMed: 10828985]

72. Pfitzner U, Odenwals A, Ostermann T, Weingard L, Ludwig B, Richter OH. Cytochrome *c* oxidase (heme aa_3) from *Paracoccus denitrificans*: Analysis of mutations in putative proton channels of subunit I. J. Bioenerg. Biomembr 1998;30:89–97. [PubMed: 9623810]

73. Blomberg MRA, Siegbahn PEM, Wikström MKF. Metal-bridging mechanism for O-O bond cleavage in cytochrome *c* oxidase. Inorg. Chem 2003;42:5231–5243. [PubMed: 12924894]

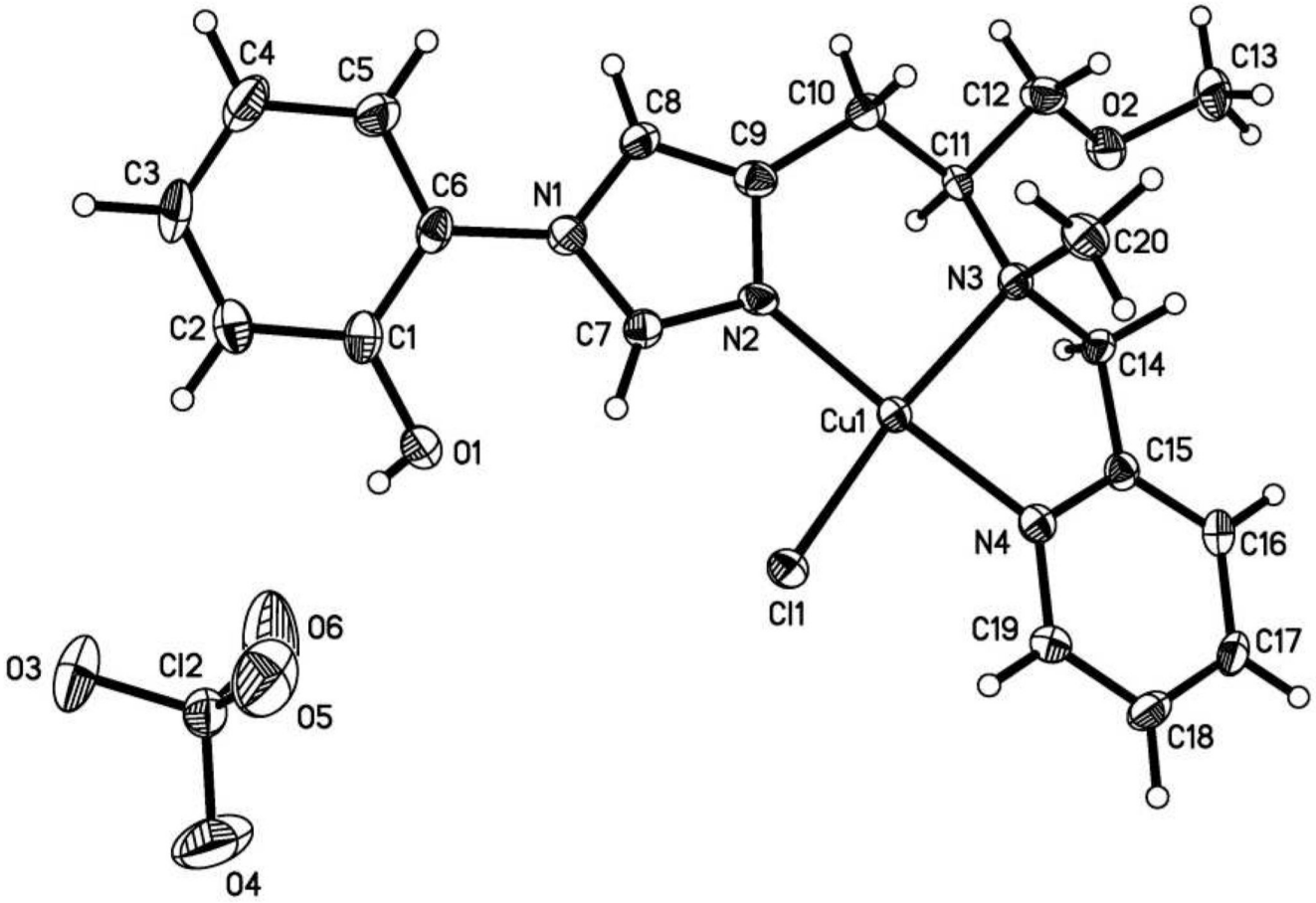

Figure 1.
X-ray crystal structure of the ^{13}C-labled Cu-complex.

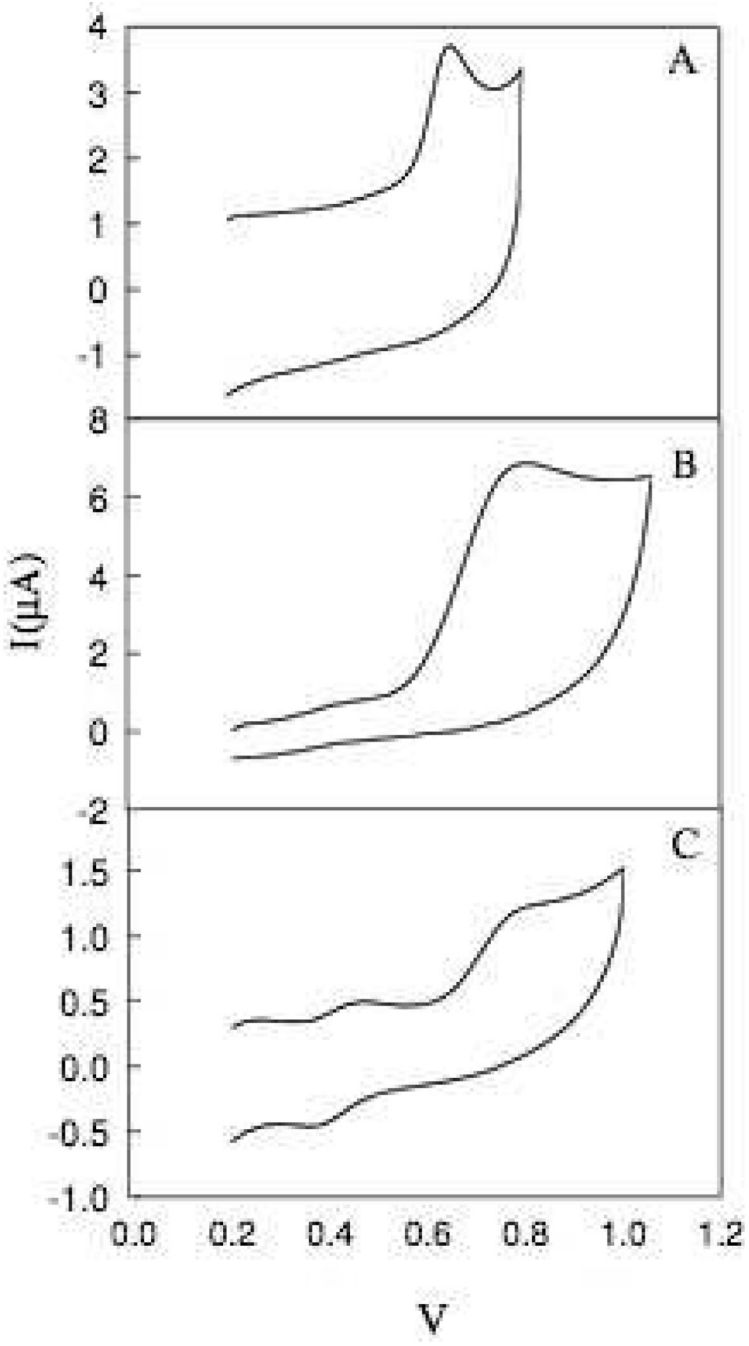

Figure 2.

Cyclic voltammograms of the natural abundance tyrosine (A), ligand (B) and Cu-complex (C). The electrochemical experiments were carried out with a CH Instrument 440 electrochemical workstation at room temperature using a glassy carbon working electrode, Ag/AgCl (saturated with 0.1 M KCl) reference electrode and a platinum wire counter electrode.[51] The experiments were carried out in the presence of 10 mM Na-phosphate pH 7.0 (0.2 M KCl).

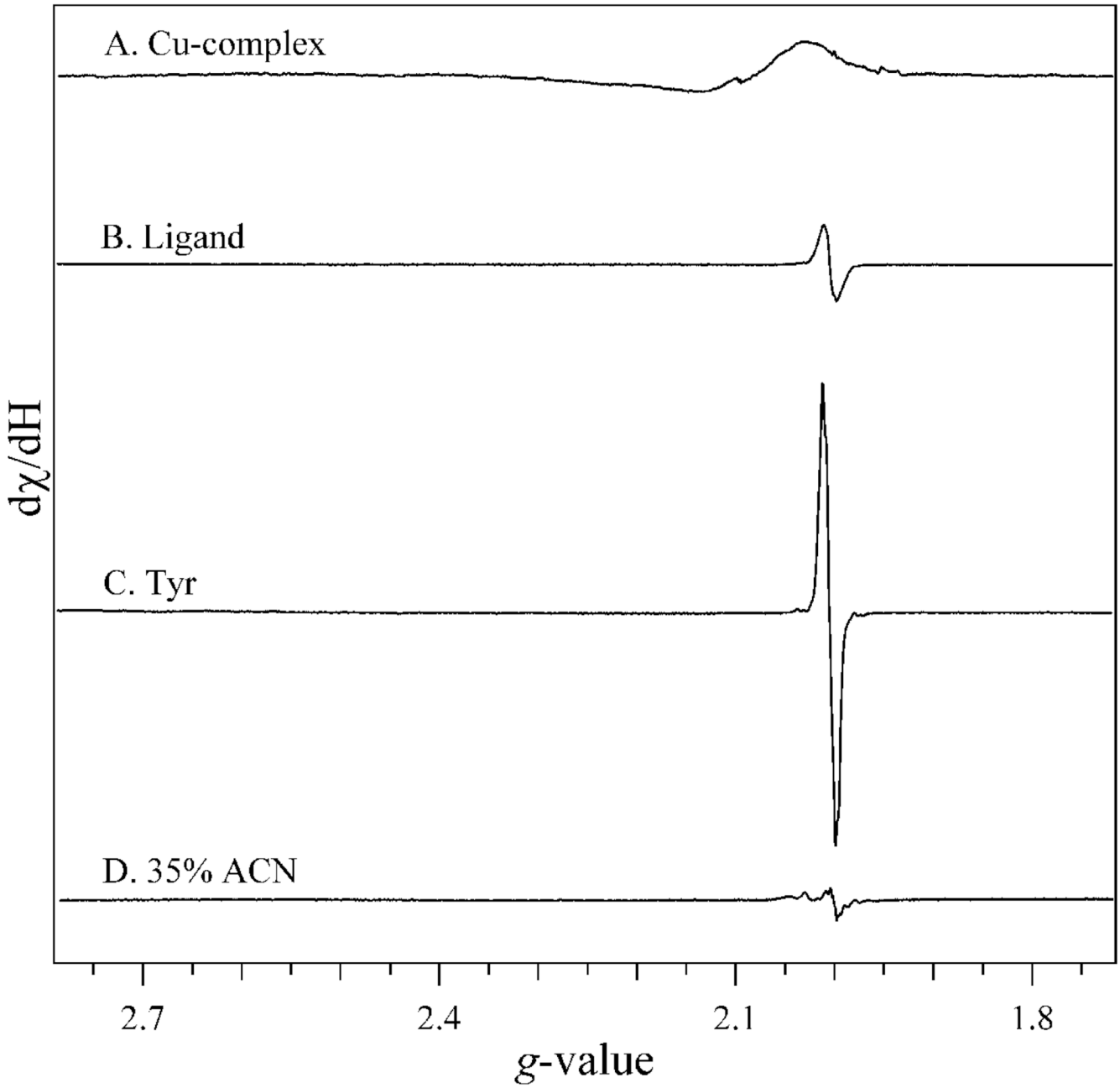

Figure 3.
EPR spectra of radicals generated by UV photolysis of (A) the Cu-complex, (B) the ligand, and (C) tyrosinate. Panel D shows the results of photolysis of a buffer blank, containing 35% acetonitrile in 10 mM Tris buffer. To generate these data (A–D), the spectrum obtained before photolysis was subtracted from one obtained after photolysis. The temperature was 100 K (see Materials and Methods for details). In (A and B), eight trials were averaged, and in (C and D), four trials were averaged.

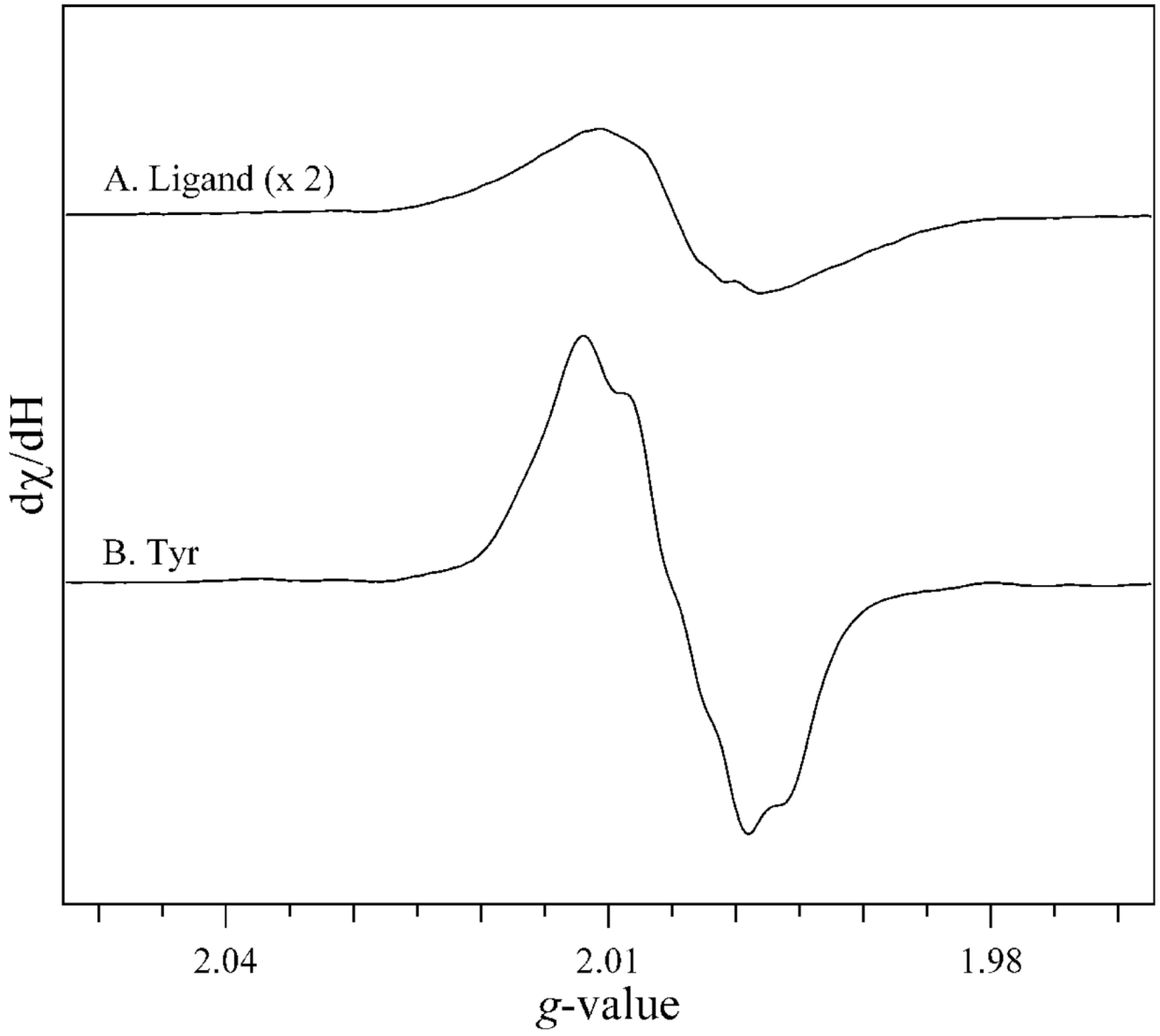

Figure 4.
EPR spectra of radicals generated by UV photolysis of (A) the ligand and (B) tyrosinate. The spectra are reproduced from Figure 3B and C, respectively, but on an expanded scale. For presentation purposes, in this figure the spectrum for the ligand (Figure 3A) is multiplied by a factor of 2. The temperature was 100 K (see Materials and Methods section and Figure 3 legend.

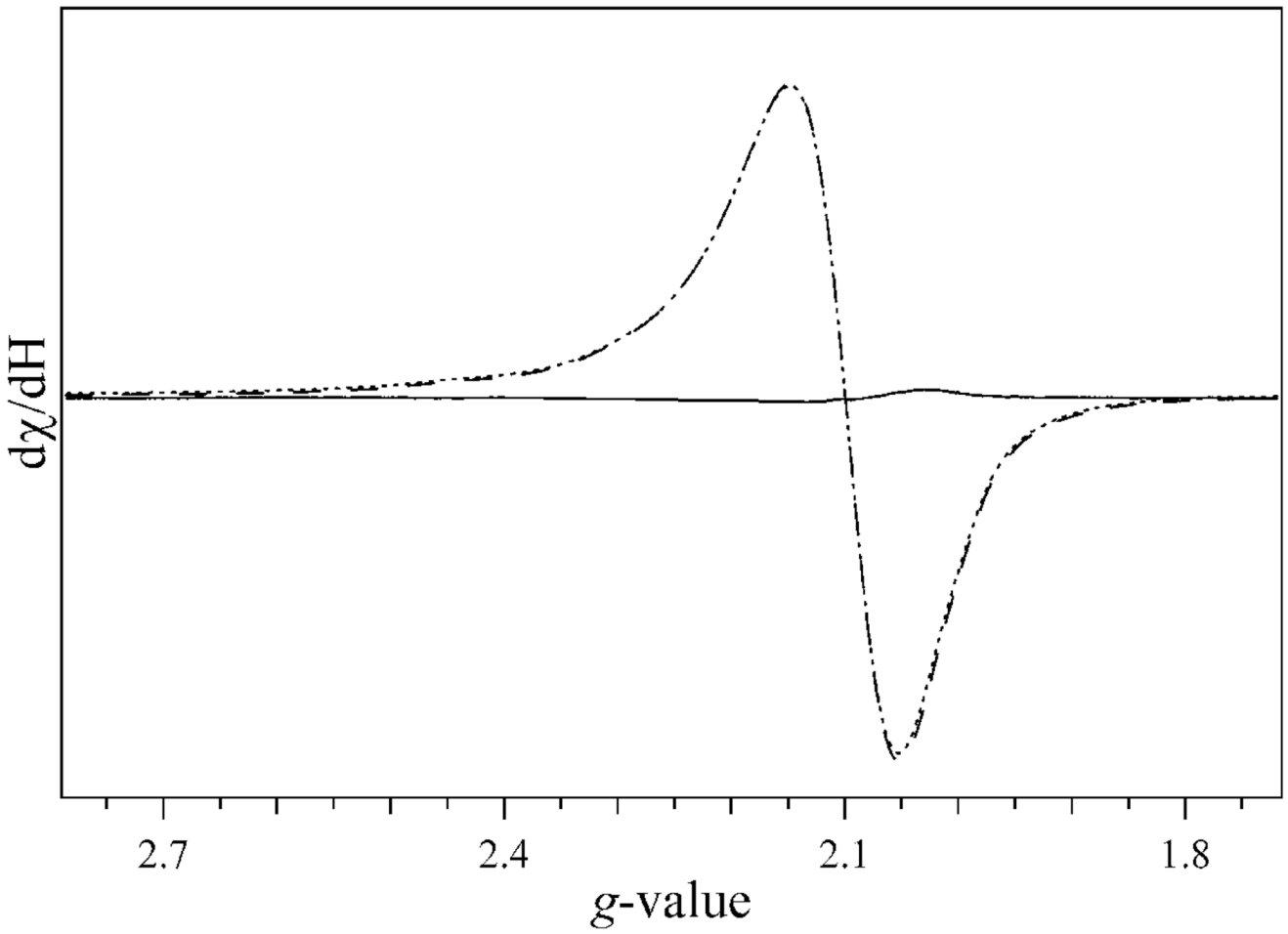

Figure 5.
EPR spectra generated before (dashed line) and after (dotted line) photolysis of the Cu-complex. The temperature was 100 K (see Materials and Methods section and Figure 3 legend). The spectrum shown in the solid line is the after photolysis-minus-before photolysis difference spectrum **(repeated from Figure 3A).** To generate the final data, eight trials were averaged.

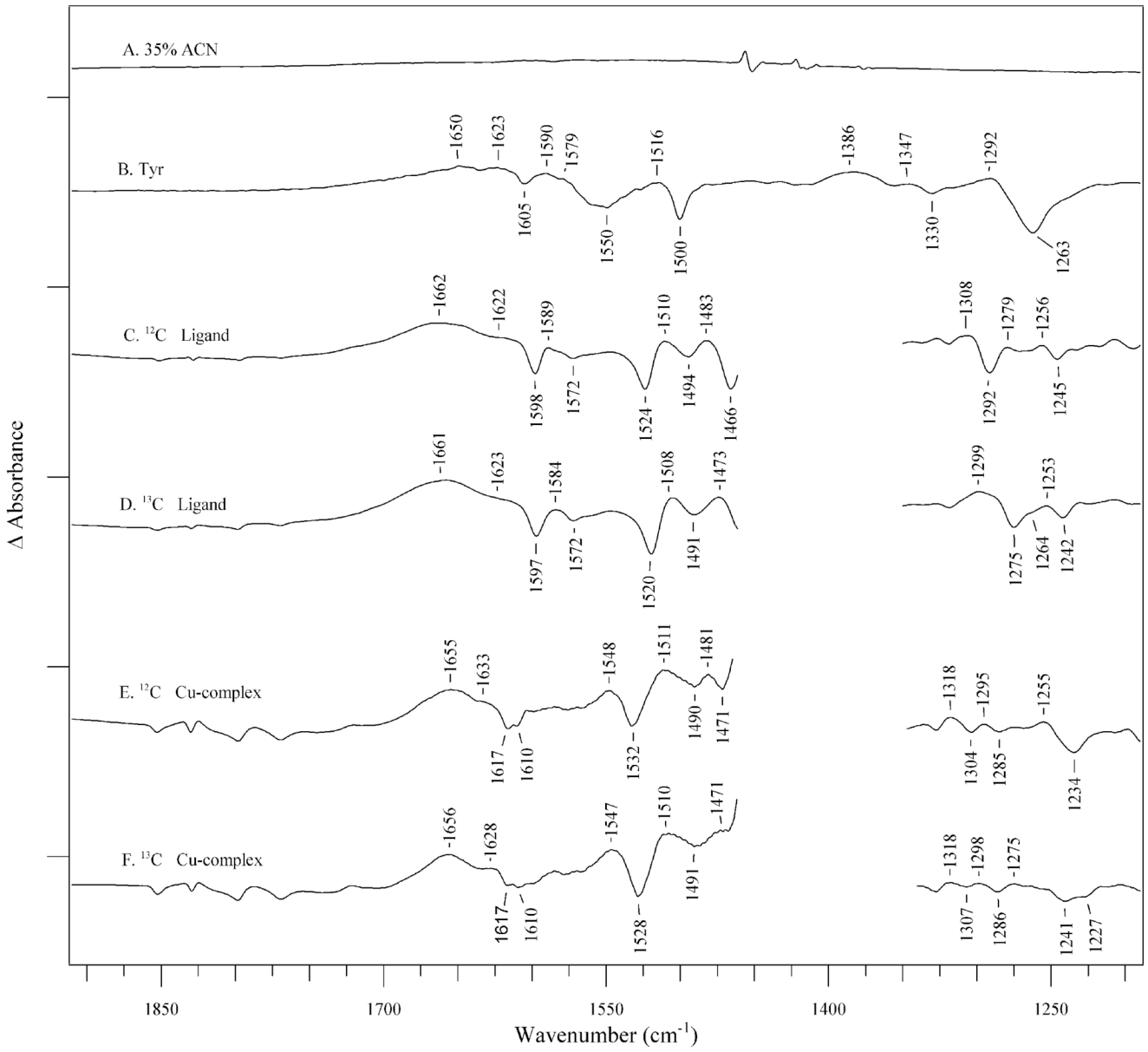

Figure 6.

Photolysis-induced difference FT-IR spectra recorded from: (A) a blank (35% acetonitrile in 10 mM Tris buffer), (B) tyrosinate, (C) natural abundance ligand, (D) ^{13}C ligand, (E) natural abundance Cu-complex, and (F) ^{13}C Cu-complex. The temperature was 79 K (see Materials and Methods for details). The spectral region between 1460 – 1350 cm^{-1} region in (B–E) was removed due to acetonitrile absorption. The final spectra are derived from 1 (A), 5 (B), 8 (C), 9 (D), 24 (E) or 23 (F) different trials. Tick marks on the *y*-axis correspond to 22.5 × 10^{-3} absorbance unit.

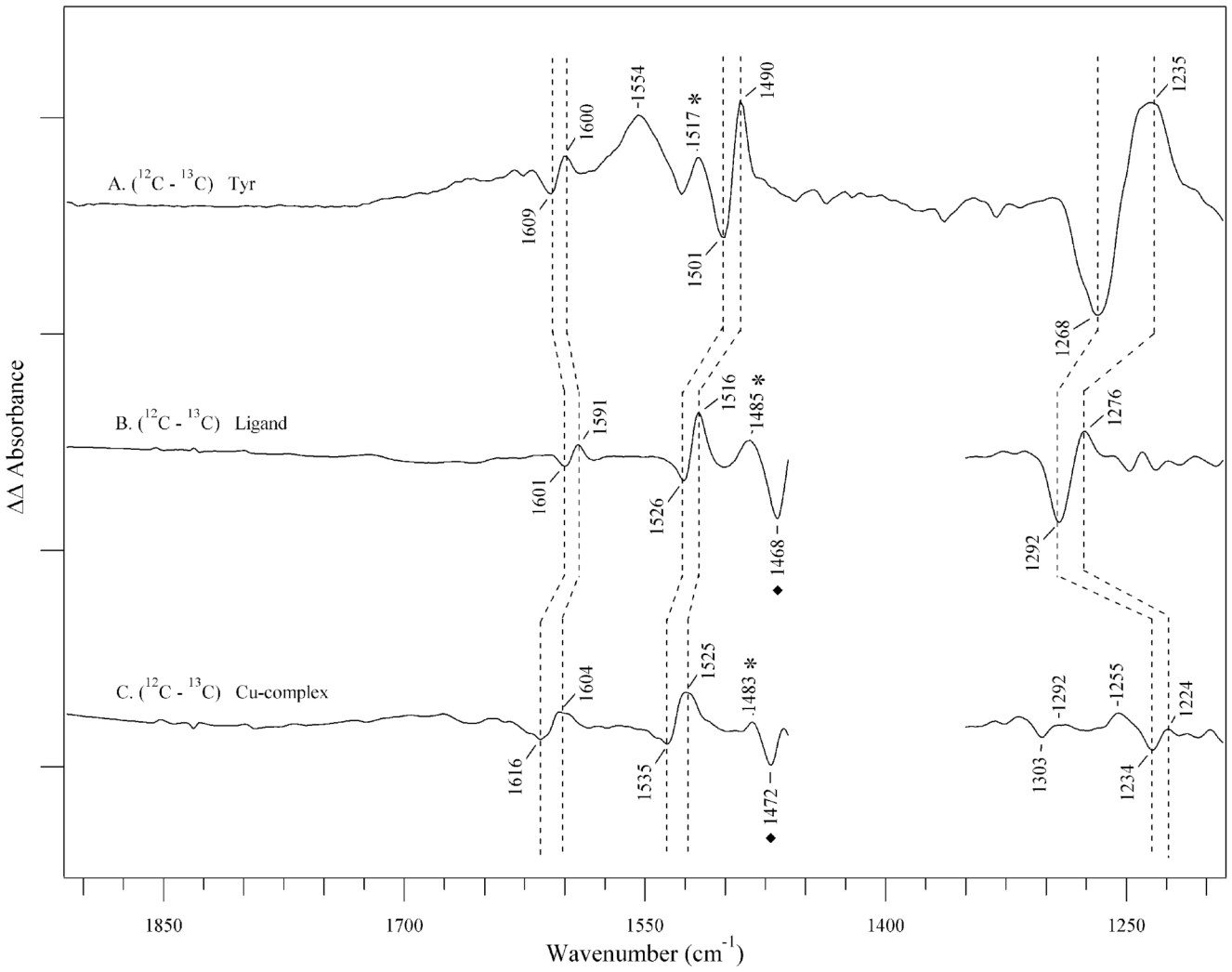

Figure 7.

Isotope-edited, ^{12}C (light – dark) -minus-^{13}C (light – dark), FT-IR spectra, showing vibrational bands sensitive to ^{13}C labeling. The data were derived from tyrosinate (7A), the ligand (7B), and the Cu-complex (7C). The ^{12}C-minus-^{13}C isotope-edited FT-IR spectrum of the ligand (B) is the subtraction of Figure 6D from 6C. The ^{12}C-minus-^{13}C istope-edited FT-IR spectrum of the Cu-complex (C) is the subtraction of Figure 6F from 6E. Tick marks on the *y*-axis correspond to 15×10^{-3} absorbance unit. The spectral region between 1460 – 1350 cm^{-1} region in (B–E) was removed due to acetonitrile absorption. The tyrosinate spectrum (A) was reproduced from reference.[52]

Table 1

Comparison of bond lengths and angles at C1’

C^{13}					
O(1)-C(1)	1.355(5)	C(1)-C(2)	1.398(6)	C(1)-C(6)	1.394(5)
O(1)-C(1)-C(6)	118.9(3)	O(1)-C(1)-C(2)	122.6(4)	C(6)-C(1)-C(2)	118.5(4)

C^{12}					
O(1)-C(1)	1.358(3)	C(1)-C(2)	1.395(4)	C(1)-C(6)	1.403(4)
O(1)-C(1)-C(6)	118.7(2)	O(1)-C(1)-C(2)	122.7(2)	C(2)-C(1)-C(6)	118.7(2)

Table 2

Assignments of Vibrational Frequencies[a] with ^{13}C Isotope Shifts

Tyrosinate[b]		Ligand		Cu-complex		
	(Δexp[c], Δcalc[d])		(Δexp[c])		(Δexp[c])	Assignment
1609	−9, −6	1601	−10	1616	−12	ν8a
1501	−11, −9	1526	−10	1535	−10	ν19a
1268	−33, −24	1292	−16	1234	−10	ν7a′

Tyrosyl radical•		Ligand•		Cu-complex•		
	(Δexp[c], Δcalc[d])		(Δexp[c])		(Δexp[c])	Assignment
1554	N.D.[e], 0	N.O.[f]		N.O.[f]		ν8a
1517	N.D.[e], −27	1485	−17	1483	−11	ν7a′

[a] Frequencies are in cm^{-1}. See Materials and Methods for experimental details.

[b] Tyrosinate assignments based on previous isotope-edited spectra and DFT calculations.[52, 61]

[c] This work; derived from double difference spectra (Figure 7).

[d] See ref[61]

[e] N.D., not determined.

[f] N.O., not observed